Pavement Distress Evaluation Using Fuzzy Logic and Moment Invariants

JACHING CHOU, WENDE A. O'NEILL, AND HENGDA CHENG

A novel approach of applying the theory of fuzzy sets and moment invariants to analyze pavement images is proposed in this paper. By applying the theory of fuzzy sets and calculating moment invariants from different types of distress, features are obtained. Then, a back-propagation neural network is used to classify these features. The crack density is used to obtain extent information. This approach is illustrated using randomly selected samples from NCHRP Project 1-27 video images of real cracks. Based on these samples, the feasibility of using the theory of fuzzy sets and moment invariants to classify different types of crack is proven. High accuracy of classification is also obtained.

Pavement distress surveys are one of the key components in a pavement management system (PMS). Currently, most states use manual surveys to obtain measurements of pavement distress. Manual surveys are inconsistent, costly, tedious, labor intensive, and subjective. Several researchers have investigated the use of image processing and pattern recognition techniques to achieve automated pavement distress ratings.

LITERATURE REVIEW

Previous Work in Pavement Image Processing

Baker et al. (*1*) discussed the use of image processing in pavement analysis for the Idaho Transportation Department. Caroff et al. (*2*) developed and validated the use of digital image processing in pavement distress to extract, recognize, and quantify longitudinal cracks, transverse cracks, and alligator cracks. Fukuhara et al. (*3*) introduced a Komatsu system for pavement condition surveys. Mohajeri and Manning (*4*) discussed the ARIA pavement distress image processing system. Li, Chan, and Lytton (*5*) proposed an approach to detect thin (width $<$ 1/4 inch) cracks. Ritchie, Kaseko, and Bavarian (*6*) applied neural networks to determine (recognition, high level processing) the type, severity, and extent of distress from video images in real time. Acosta, Figueroa, and Mullen (*7*) developed image processing procedures with several system components, such as image digitizing and deblurring, image segmentation and clustering, feature extraction and cluster classification, and a pavement condition rating routine. Koutsopoulos and Downey (*8*) adopted a primitive-based classification approach to classify distress type. Chua and Xu (*9*) proposed a prototype system that consists of an ordinary 8-mm camcorder, an inexpensive image-digitizing board, and an algorithm running on an IBM 486-compatible personal computer to detect pavement distress.

Departments of Civil and Environmental Engineering and Computer Science, Utah State University, Logan, Utah 84322.

In general, previous studies show that the following steps are required in pavement image processing: (*a*) image acquisition, (*b*) image enhancement, (*c*) image segmentation, and (*d*) image classification. The following sections will discuss algorithms used in research applications of using video image processing.

Moment Invariants and the Theory of Fuzzy Set in Image Analysis

Pal and King (*10*) said, "The theory of fuzzy sets provides a suitable algorithm in analyzing complex systems and decision processes when the pattern indeterminacy is due to inherent variability and/or vagueness (fuzziness) rather than randomness." There are several reasons that images are fuzzy: (*a*) images are generally ambiguous when represented by pixels because of the varied levels of brightness (0 to 255) and the lack of crisp boundaries between edges and nonhomogeneous regions; (*b*) information is lost in the transformation from a three-dimensional image to a two-dimensional image; and (*c*) ambiguity and vagueness in interpreting results from low level image processing. So the use of fuzzy set theory may be more suitable than ordinal set theory for an image-processing problem.

Pal (*11*) introduced an index of fuzziness and entropy as a quality index of enhanced images. In Pal and Ghosh's work (*12*), fuzzy geometry is used in image analysis. Pal and Rosenfeld (*13*) proposed image enhancement and thresholding by optimizing the compactness of fuzziness. Linear index of fuzziness, quadratic index of fuzziness, entropy, and index of nonfuzziness are also introduced. Pal, King, and Hashim (*14*) used fuzzy sets to describe images and to extract primitives. Keller and Carpenter (*15*) used fuzzy set theory to segment images. Zhao, Li, and Cheng (*16*) applied a fuzzy logic approach to image enhancement. Huntsberger, Jacobs, and Cannon (*17*) have developed an iterative fuzzy clustering technique based on a fuzzy c-means algorithm for image segmentation.

Moments and functions of moments have been applied as pattern features in several applications to recognize objects. Hu (*18*) introduced moment invariants based on algebraic invariants. Noll (*19*) discussed some general properties of Zernike polynomials, such as their Fourier transforms, integral representations, and derivatives. Reddi (*20*) introduced radial and angular moments, which are more general in moment functions compared with Hu's moment invariants. Teague (*21*) introduced Zernike moments based on the theory of orthogonal polynomials and Legendre moments based on Legendre polynomials. In Teague's research (*22*), moments with arbitrarily high orders were developed. In 1984 (*23*) and 1985 (*24*), Abu-Mostafa and Psaltis introduced complex moments as a simple and straightforward way to derive moment invariants. Maitra (*25*) found that moments are not contrast invariant between two images.

Hsia (*26*) discussed moment variations due to numerical integration and interpolation in digital images.

Previous efforts show that moment invariants and the theory of fuzzy sets have been successfully applied to image processing and analysis for a variety of applications. These applications include recognition of hand-printed characters, aircraft identification, interpretation of ship photos, recognition of vehicle images, and others. Preliminary results from Chou's work (*27,28*) show that: (*a*) fuzzy image-processing techniques can provide a better approach to process pavement images; and (*b*) by the properties of moment invariants under change of size (scale), change of position (translation), change of orientation (rotation), and reflection, cracks' features can be extracted, and cracks can be correctly classified.

This paper focuses on models and algorithms for automated asphalt pavement image processing. Algorithms of image preprocessing, image enhancement, image segmentation, distress feature extraction and classification, and obtaining extent information are presented.

METHODOLOGY

Pavement Image Acquisition and Digitization

Sample images for this work were provided by the NCHRP, Project 1-27. Images were digitized using a Panasonic S-VHS AG-7500 editing machine controlled by a DIAQUEST board in an IBM compatible personal computer and a TARGA+ image-digitizing board. The image size for each frame is 482 × 512 pixels, and the gray scale is from 0 to 255.

Pavement Image Preprocessing

Because of the nonuniform illumination, some images' right and left portions are darker than their central area. Figure 1 shows this situation in a nondistress image. In this case, a nonlinear equation is used to adjust the image histogram. This equation is

$$f(x,y) = f(x,y) + \begin{cases} p_1 \times \sqrt{x_b - x_i} & 0 \le x_i \le x_b \\ 0 & x_b < x_i \le x_e \\ p_2 \times \sqrt{x_i - x_e} & x_e < x_i \le 255 \end{cases} \quad (1)$$

where

x_i = current x-position,
x_e = position where the right dark area begins,
x_b = position where the left dark area ends, and
p_1, p_2 = parameters.

The values of x_e and x_b are derived from 45 sample images. The values of p_1 and p_2 are calibrated from 45 sample images by manually examining images. In practical situations, these parameters can be calibrated from field images and used for the remaining pavement images because the lighting condition is under control. This step is only required when images are darker along the edges.

Pavement Image Rotation

To generate enough image samples and test moment invariants under rotation for pavement distress images, a rotating technique is used. This technique is referred to as a geometric transformation. In this transformation the relationship between a source image and a rotated image is

$$\begin{bmatrix} x_{new} \\ y_{new} \end{bmatrix} = \begin{bmatrix} \cos\theta & \sin\theta \\ -\sin\theta & \cos\theta \end{bmatrix} \times \begin{bmatrix} x_{old} \\ y_{old} \end{bmatrix} \quad (2)$$

According to Lindley (*29*), to guarantee one-to-one mapping of source to rotated pixels, reverse mapping is used. Interpolation is used to calculate the coordinates for the pixels whose locations are fractional during the rotating process. Bi-linear interpolation is used here.

The relationship between $f(x,y)$ and the four surrounding points is described in Figure 2 as follows.

$$\begin{aligned} j &= \text{INT}[x] \qquad \alpha = x - y \\ k &= \text{INT}[y] \qquad \beta = y - k \end{aligned} \quad (3)$$

where INT[] is an integer function.

In Y-direction,

$$\begin{aligned} A &= (1 - \beta) * f(j, k) + \beta * f(j, k + 1) \\ B &= (1 - \beta) * f(l, k) + \beta * f(j + 1, k + 1) \end{aligned} \quad (4)$$

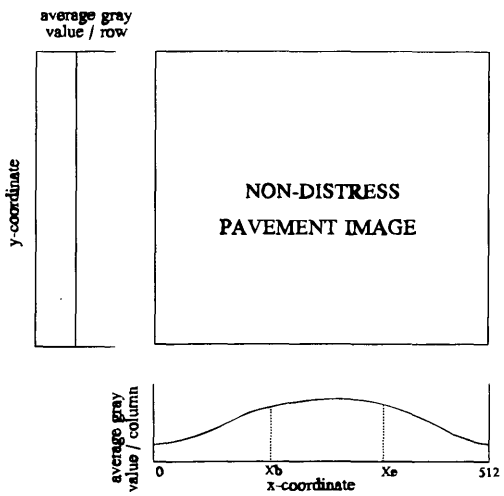

FIGURE 1 Nonuniform illumination in a nondistress pavement image.

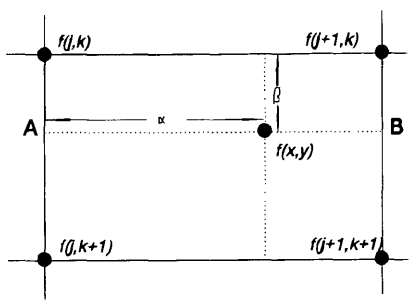

FIGURE 2 Bilinear interpolation in image rotation.

In X-direction,

$$f(x,y) = \alpha * \beta + (1 - \alpha) * A \tag{5}$$

Finally,

$$f(x,y) = (1 - \alpha)(1 - \beta) * f(j, k) + \alpha(1 - \beta) f(j+ 1, k) + \beta (1 - \alpha) * f(j, k + 1) + \alpha\beta f(j + 1, k + 1) \tag{6}$$

when $\alpha = \beta = 0, f(x, y) = f(j, k)$.

Pavement Image Enhancement

Zhao et al. (*16*) used a fuzzy algorithm to enhance images. In this research, a Z-function is used instead of S-function because the S-function is typically used for bright objects, and pavement cracks are dark. First, a function complementary to the S-function [i.e., (1-S)-function] is used. The Z-function is defined as

$$Z(x,a,b,c) = \mu_x(x) = \begin{cases} 1 & x < a \\ 1 - \dfrac{(x-a)^2}{(b-a)(c-a)} & a \le x < b \\ \dfrac{(x-c)^2}{(c-b)(c-a)} & b \le x < c \\ 0 & x \ge c \end{cases} \tag{7}$$

where

a and c = parameters determining the fuzzy region and associated with the histogram of the gray scale of the image,
$b = (a + c)/2$, and
$\times$ = pixel value.

Second, an averaging filter is used to remove noise, thus smoothing the image. And the output is $v(m,n)$. The definition of $v(m,n)$ is

$$v(m,n) = \text{average } [\mu_x(m - k, n - l), (k,l) \in W)] \tag{8}$$

where W is the averaging filter window, and its size is 3×3. Third, a transformation function (T) is used to enhance the image in the fuzzy domain. The transformation function is

$$\mu'_x(x_{mn}) = T[\, v(m,n)]$$

$$= \begin{cases} 2 \times [v(m,n)]^2 & 0.0 \le v(m,n) < 0.5, \\ 1 - 2 \times (1 - v[m,n)]^2 & 0.5 \le v(m,n) < 1.0 \end{cases} \tag{9}$$

Finally, fuzzy membership values are converted to gray-level values.

Pavement Image Thresholding

A fuzzy thresholding technique based on the principle of maximum fuzzy entropy is used. The degree of ambiguity of an image can be measured by the entropy of a fuzzy set. A threshold is obtained by maximizing the fuzzy entropy of an image. The fuzzy entropy is defined as

$$H(x_i) = \frac{-1}{M\,N\,(\ln 2)} \sum_{x=L_{\min}}^{L_{\max}} \{\mu_x(x_i) \ln[\mu_x(x_i)] + [1 - \mu_x(x_i)] \ln[1 - \mu_x(x_i)]\} \times h(x_i) \tag{10}$$

where $h(x)$ is the histogram. After thresholding, a binary image is obtained.

Pavement Image Feature Extraction

There are seven types of distress that are considered in this research. These distresses are longitudinal cracks, transverse cracks, combined longitudinal and transverse cracks, right and left diagonal cracks, alligator (fatigue) cracks, and nondistress. Let $f(m,n)$ be the function of distress in a segmented image R containing M by N pixels and first order moments of the centroid of the shape,

$$M_{p,q} = \sum_m \sum_n m^p n^q f(m,n)$$

$$\overline{m} = \frac{M_{1,0}}{M_{0,0}} = \frac{1}{M * N} \sum \sum m f(m,n)$$

$$\overline{n} = \frac{M_{0,1}}{M_{0,0}} = \frac{1}{M * N} \sum \sum n f(m,n) \tag{11}$$

where $f(m,n) = 1$ for binary images. The moment-based features include the following.

Hu Moments

Hu's approach was proposed in 1962 (*18*). The seven moments up to three orders are

$$\begin{aligned}
HM_1 &= \eta_{2,0} + \eta_{0,2} \\
HM_2 &= (\eta_{2,0} + \eta_{0,2})^2 + 4\eta_{1,1}^2 \\
HM_3 &= (\eta_{3,0} + 3\eta_{1,2})^2 + (3\eta_{2,1} - \eta_{1,2})^2 \\
HM_4 &= (\eta_{3,0} + \eta_{1,2})^2 + (\eta_{2,1} + \eta_{0,3})^2 \\
HM_5 &= (\eta_{3,0} - 3\eta_{1,2})(\eta_{3,0} + \eta_{1,2})[(\eta_{3,0} + \eta_{1,2})^2 - 3(\eta_{2,1} + \eta_{0,3})^2] \\
&\quad + (3\eta_{2,1} - \eta_{0,3})(\eta_{2,1} + \eta_{0,3})[3(\eta_{3,0} + \eta_{1,2})^2 - (\eta_{2,1} + \eta_{0,3})^2] \\
HM_6 &= (\eta_{2,0} - \eta_{0,2})[(\eta_{3,0} + \eta_{1,2})^2 - (\eta_{2,1} - \eta_{0,3})^2] \\
&\quad + 4\eta_{1,1}(\eta_{3,0} + \eta_{1,2}) + (\eta_{2,1} + \eta_{0,3}) \\
HM_7 &= (3\eta_{2,1} - \eta_{3,0})(\eta_{3,0} + \eta_{1,2})[(\eta_{3,0} + \eta_{1,2})^2 \\
&\quad - 3(\eta_{2,1} + \eta_{0,3})^2] + (3\eta_{1,2} \\
&\quad - \eta_{3,0})(\eta_{2,1} + \eta_{0,3})[3(\eta_{3,0} + \eta_{1,2})^2 - (\eta_{2,1} + \eta_{0,3})^2]
\end{aligned} \tag{12}$$

where $n_{p,q} = \sum_m \sum_n (m - \overline{m})^p (n - \overline{n})^q f(m,n)$

Bamieh Moments

The Bamieh moment (*30*) can be expressed by using central moments as shown

$$\begin{aligned}
BM_1 &= \eta_{02}\eta_{20} - \eta_{11}^2 \\
BM_2 &= (\eta_{03}\eta_{30} - \eta_{21}\eta_{12})^2 - 4(\eta_{03}\eta_{12} - \eta_{21}^2)(\eta_{21}\eta_{30} - \eta_{12}^2) \\
BM_3 &= \eta_{40}\eta_{04} - 4\eta_{31}\eta_{13} + 3\eta_{22}^2 \\
BM_4 &= \eta_{40}\eta_{22}\eta_{04} - 2\eta_{31}\eta_{22}\eta_{13} - \eta_{40}\eta_{13}^2 - \eta_{04}\eta_{31}^2 - \eta_{22}^3
\end{aligned} \tag{13}$$

Zernike (Teague) Moments

The Zernike moments (*21*) expressed in terms of usual moments are:

$$ZM_1 = \frac{3}{\pi}\,[2 \times (\eta_{20} + \eta_{02}) - 1]$$

$$ZM_2 = \frac{9}{\pi^2}\,[(\eta_{20} - \eta_{02})^2 + 4(\eta_{11})^2]$$

$$ZM_3 = \frac{16}{\pi^2}\,[(\eta_{03} - 3\eta_{21})^2 + (\eta_{30} - 3\eta_{12})^2]$$

$$ZM_4 = \frac{144}{\pi^2}\,[(\eta_{03} + \eta_{21})^2 + (\eta_{30} + \eta_{12})^2]$$

$$ZM_5 = \frac{13824}{\pi^4}\,[(\eta_{03} - 3\eta_{21})(\eta_{03} + \eta_{21}) \times [(\eta_{03} + \eta_{21})^2 - 3(\eta_{30} + \eta_{12})^2] - (\eta_{30} - 3\eta_{12})(\eta_{30} + \eta_{12}) \times [(\eta_{30} + \eta_{12})^2 - 3(\eta_{03} + \eta_{21})^2]\}$$

$$ZM_6 = \frac{864}{\pi^3}\,\{(\eta_{02} - \eta_{20})[(\eta_{30} + \eta_{12})^2 - [(\eta_{30} + \eta_{21})^2] + 4\eta_{11}(\eta_{03} + \eta_{21}) \times (\eta_{30} + \eta_{12})\} \quad (14)$$

Pavement Image Classification

A backpropagation neural network is used to classify the type of distress based on Hu's seven moment invariants (HM), Zernike's six moment invariants (ZM), and Bamieh's four moment invariants (BM). There are 18 nodes: 4 for BM, 7 for HM, 6 for ZM, and 1 for bias in the input layer, 17 nodes in the hidden layer, and 7 nodes in the output layer to represent seven different types of cracks.

Extent of Pavement Distress

Crack density (D_P) is used as an index of extent in this paper. Originally, the crack density is defined as

$$D_P(\text{crack density}) = \frac{P_M}{P_N} \quad (15)$$

where P_M is the number of distress pixels, and P_N is the total number of image pixels. For example, if the number of distress pixels is 20,000, and the number of total image pixels is 246,784 (482 × 512), then the crack density is 8.1 percent (20,000/246,784 · 100 percent).

Simply using the number of pixels to calculate the crack density causes errors. For example, in a longitudinal crack with broken line segments some pixels are missing in the crack density calculation, and the calculated crack density will be smaller than the actual one. In this paper a modified crack density is used. By assuming that there are B_N numbers of total image blocks in an image and B_M numbers of image blocks containing distress, the crack density (D_B) is defined as

$$D_B(\text{crack density}) = \frac{B_M}{B_N} \quad (16)$$

The modified crack density can prevent problems associated with missing pixels due to image processing.

Image blocks are generated by partitioning a binary pavement image into certain regions. The mean and the variance of the pixel values within each image block are used to determine the existence of distress in that block. For example, if the size of image and image block is 482 × 512 and 48 × 48, respectively, then there are 121 blocks in an image. The crack density is 9.1 percent (11/121 · 100 percent) if there are 11 blocks containing distress.

The relationship between the crack density and a density rating (extent) is shown on Table 1. From this table, an image with crack density between 41 and 80 percent will receive an integer rating of 5 (Table 1).

To reasonably interpret extent of pavement distress using the crack density, the crack density of alligator cracks are treated differently from the other types of distress. With the same crack density value alligator cracks should have a higher extent rating. Alligator cracks are "area" (two-dimensions) types of cracks, and longitudinal and transverse cracks are linear.

There are two ways to handle this problem. Different criteria may be used to select distress image blocks. Otherwise, different density rating tables may be used for alligator cracks but the same criteria in deciding distress image blocks. In this paper, the former approach is used.

RESULTS

Pavement Image Preprocessing

This step is only required when images are darker in the edges. The values of x_e and x_b are derived from 45 sample images. The values of p_1 and p_2 are calibrated from 45 sample images by "trial and error." The results are: p_1 is 2.0, p_2 is 4.0, x_e is 430, and x_b is 100.

Pavement Image Enhancement and Thresholding

Originally 18 combinations of transverse and longitudinal crack images, 14 longitudinal crack images, 13 alligator crack images, 7 transverse crack images, and 7 nondistress images were used. Left and right diagonal cracks were generated by rotating longitudinal and transverse cracks with 45 degrees and 135 degrees, respectively. These original images were rotated by 0.5, 1.0, 1.5, 2.0, 358.0, 358.5, 359.0, and 359.5 degrees to generate more test samples.

Because of nonuniform illumination and background noise in NCHRP images, different a, b, and c values in the Z-membership function are related to the histogram of the images and can be determined by experimentation. In thresholding, the maximum entropy

TABLE 1 The Density Rating

Rate	Density range
0	less than 1%
1	1% to 5%
2	6% to 10%
3	11% to 20%
4	21% to 40%
5	41% to 80%
6	81% to 100%

approach is used to determine threshold values for adaptively thresholding subimages. Two subimages of 256 × 256 and two subimages of 226 × 256 are processed.

Pavement Image Feature Extraction

Moment features based on Bamieh's, Hu's, and Zernike's moments were calculated. Moment values were computed in the format of logarithms with base 10, and then they were normalized and input to the neural network. Figures 3–7 show the result of image processing for longitudinal cracks, transverse cracks, combined longitudinal and transverse cracks, alligator cracks, and nondistress, respectively.

Pavement Image Classification

A backpropagation neural network was used to classify different types of cracks. Figure 8 shows the structure of this neural network.

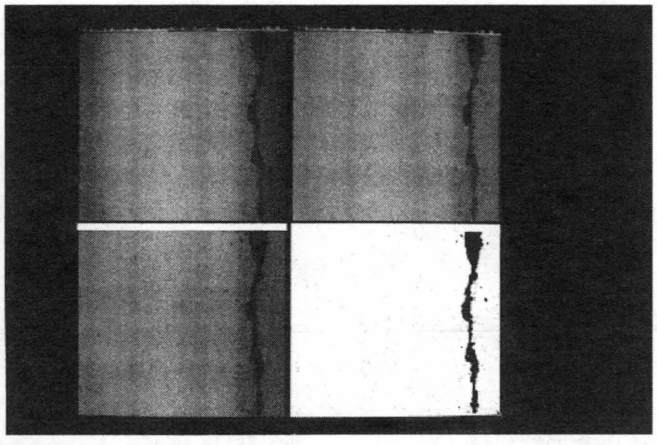

FIGURE 3 Results of longitudinal cracks after image processing (*top left*: original image; *top right*: preprocessed image; *bottom left*: enhanced image; *bottom right*: binary image).

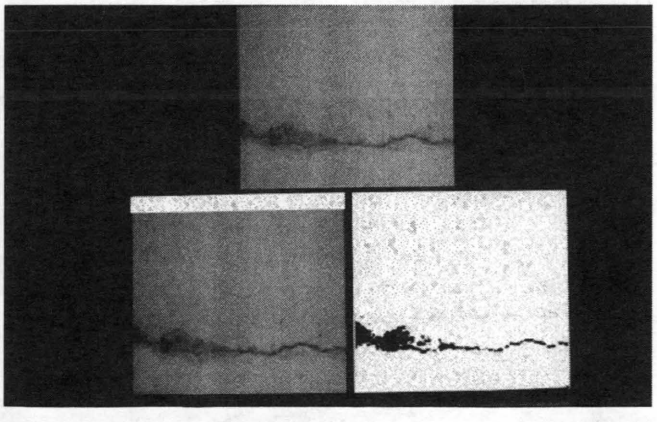

FIGURE 4 Results of transverse cracks after image processing (This image does not require preprocessing) (*top*: original image; *bottom left*: enhanced image; *bottom right*: binary image).

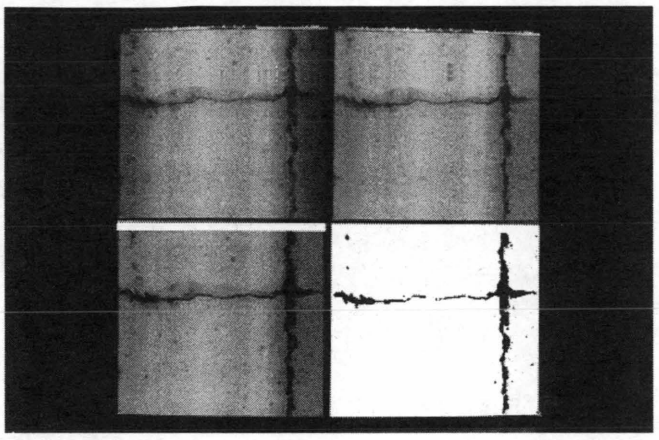

FIGURE 5 Results of combined longitudinal and transverse cracks after image processing (*top left*: original image; *top right*: preprocessed image; *bottom left*: enhanced image; *bottom right*: binary image).

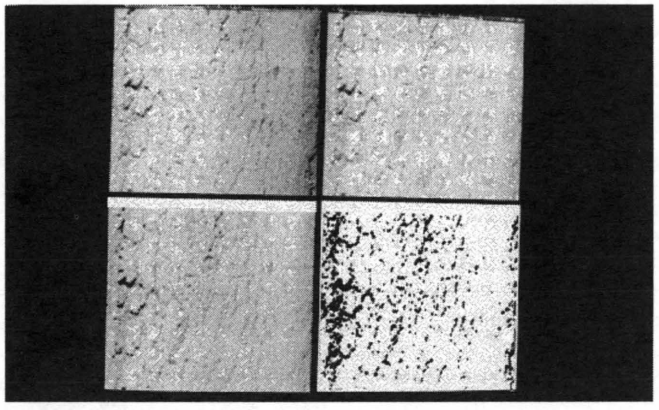

FIGURE 6 Results of alligator after image processing (*top left*: original image; *top right*: preprocessed image; *bottom left*: enhanced image; *bottom right*: binary image).

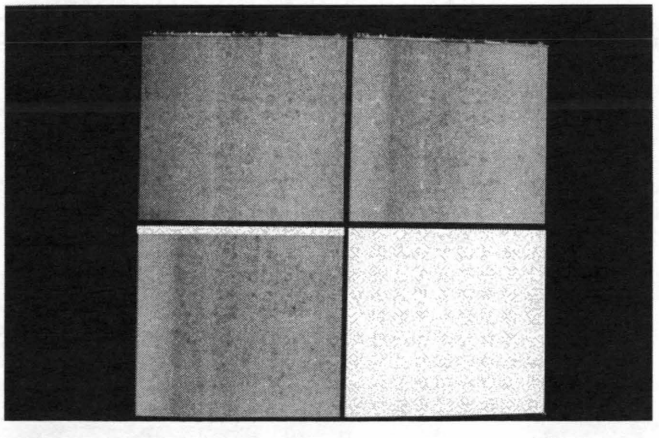

FIGURE 7 Results of nondistress after image processing (*top left*: original image; *top right*: preprocessed image; *bottom left*: enhanced image; *bottom right*: binary image).

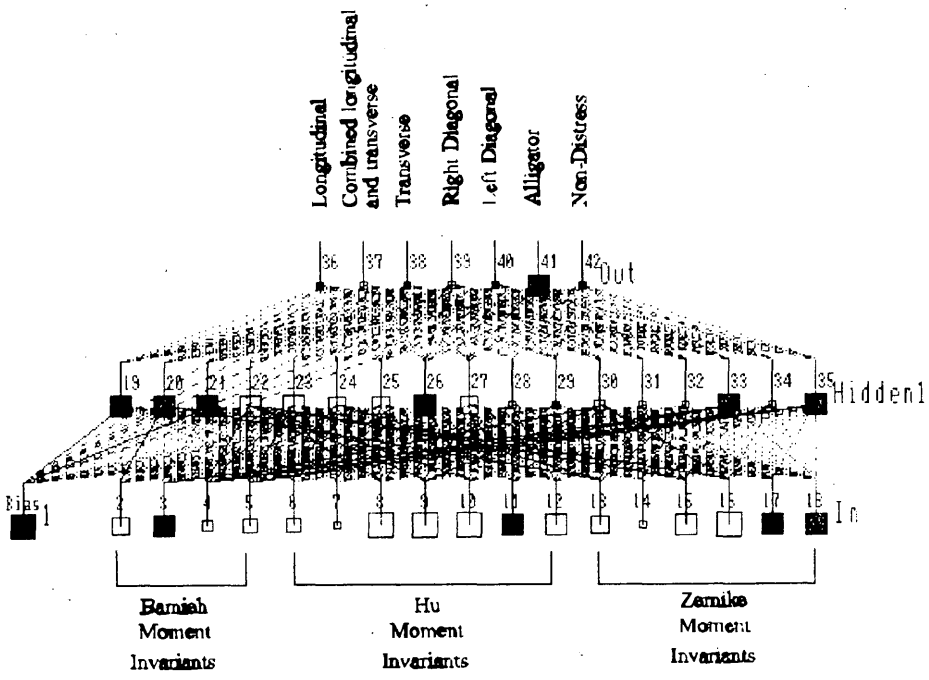

FIGURE 8 The structure of a backpropagation neural network (this figure is generated from NeuralWork's NeuralWare software simulator).

TABLE 2 Comparison of Classification Accuracy

	Chua	Lee	Ritchie	Acosta	Mohajeri	Koutsopoulos	This Research
Transverse	100%	50%[a]	93%	——	——	100%	100%
Longitudinal	100%	100%	96%	——	——	100%	100%
Diagonal	93%	——	——	——	——	——	100%
Alligator	80%	67%	——	——	——	73%	100%
Block	67%	——	——	——	——	33%	——
Combined of longitudinal and transverse	——	——[b]	——	——	——	——	100%
Non-Distress	75%	——	99%	——	——	——	100%
Combined distress	——	——	60%	——	——	——	——
Overall	——	——	——	90%	95%	——	100.00%

[a] Two transverse cracks in an image were considered as transverse cracks here.
[b] These were combinations of longitudinal and transverse cracks. Since there was no template for this type in this paper, it will not be counted here.

TABLE 3 Computation Time Required in Each Step for the Same Image

Procedures	Time required
Image preprocessing	1.5 sec
Image enhancement	9.8 sec
Image segmentation	6.2 sec
Moment calculation	7.8 sec
Neural network classifier	< 1 sec
Total time required	35.3 sec

A total of 126 longitudinal cracks (Class 1), 162 combined longitudinal and transverse cracks (Class 2), 78 transverse cracks (Class 3), 126 right diagonal cracks (Class 4), 126 left diagonal cracks (Class 5), 117 alligator cracks (Class 6), and 42 nondistress (Class 7) were generated. During the learning process, 108 Class 1 samples, 135 Class 2 samples, 68 Class 3 samples, 108 Class 4 samples, 108 Class 5 samples, 99 Class 6 samples, and 36 Class 7 samples were used. The remaining samples were used as the test data. The competition approach (win-and-take) was applied, which means the largest output value in the seven neural output nodes determines the type of distress. For example, a sample is classified as an alligator crack if Node 6 has the largest value.

Table 2 shows the classification result. Every type of distress is classified correctly for these test images used in this research. In terms of computational efforts, Table 3 shows the average computation time required for each step for a single image. This algorithm was implemented using the C language in IBM RS-6000 machine.

Extent of Pavement Distress

The mean and the variance of the pixels within each image block are used to determine the extent of distress in an image block. The size of the image block used in this experiment was 48 × 48 pixels. In alligator cracks distress is evaluated if the mean is smaller than 245 and the variance is greater than 0. For other types of distress, distress extent is evaluated if the mean is smaller than 245 and the variance is greater than 1 (Table 2). Values of the mean (245) and the variance (0 and 1) are found by "trial and error" in this experiment. Table 4 shows results of the density rating. From Table 3, an alligator crack image with a crack density of 65 percent (Image 1)

TABLE 4 The Result of Severity Rating

Image #	Longitudinal		Combined of longitudinal and transverse		Transverse		Alligator	
	Density (%)	Extent Rating	Density (%)	Extent Rating	Density (%)	Extent Rating	Density (%)	Extent Rating
1	11	3	25	4	12	3	65	5
2	17	3	21	4	22	4	39	4
3	11	3	21	4	26	4	31	4
4	12	4	22	4	22	4	40	4
5	14	3	17	3	22	4	86	6
6	12	3	26	4	25	4	74	5
7	12	3	20	3	17	3	69	5
8	8	2	21	4	26	4	69	5
9	9	2	17	3			52	5
10	10	2	18	3			89	6
11	8	2	17	3			71	5
12	7	2	17	3			41	5
13	7	2	21	4			64	5
14	9	2	28	4				
15			23	4				
16			24	4				
17			19	3				
18			20	3				

will have an extent rating of 5, and a combined longitudinal and transverse crack with a crack density of 17 percent (Image 2) will have an extent rating of 3.

CONCLUSIONS

A fuzzy enhancement algorithm, moment invariant features, and neural networks were used to classify pavement cracks (alligator cracks, longitudinal cracks, transverse cracks, combinations of longitudinal and transverse cracks, diagonal cracks, and nondistress). Moment invariants are shown to be feasible for pavement crack classification. Although the shape of pavement crack is irregular and fuzzy, which results in the loss of invariant properties, moment invariants still perform well. The extracted features are input to the neural network, and the classification accuracy is quite satisfactory. Using different criteria in the crack density to determine severity between alligator and other types of cracks provides more reasonable results.

REFERENCES

1. Baker, J., B. Dahlstrom, K. Longenecker, and T. Buu. Video Image Distress Analysis Technique for Idaho Transportation Department Pavement Management System. *Transportation Research Record 1117*, TRB, National Research Council, Washington, D.C., 1987, pp. 159–163.
2. Caroff, G., P. Joubert, F. Prudhomme, and G. Soussain. Classification of Pavement Distress by Image Processing. *Proc., First International Conference on Applications of Advanced Technologies in Transportation Engineering*, ASCE, San Diego, Calif., 1989, pp. 46–51.
3. Fukuhara, T., K. Terada, M. Nagao, A. Kasahara, and S. Ichihashi. Automatic Pavement-Distress-Survey System. *Journal of Transportation Engineering*, ASCE Vol. 116, No. 3, 1990, pp. 280–286.
4. Mohajeri, M. H., and Patrick J. Manning, ARIA: An Operating System of Pavement Distress Diagnosis by Image Processing. *Transportation Research Record 1311*, TRB, National Research Council, Washington, D.C., 1991, pp. 120–130.
5. Li, L., P. Chan, and R. L. Lytton. Detection of Thin Cracks on Noisy Pavement Images. *Transportation Research Record 1311*, TRB, National Research Council, Washington, D.C., 1991, pp. 131–135.
6. Ritchie, S. G., M. Kaseko, and B. Bavarian. Development of an Intelligent System for Automated Pavement Evaluation. *Transportation Research Record 1311*, National Research Council, Washington, D.C., 1991, pp. 120–130.
7. Acosta, J. J. Adolfo, L. Figueroa, and R. L. Mullen. Low-Cost Video Image Processing System for Evaluating Pavement Surface Distress. *Transportation Research Record 1348*, TRB, National Research Council, Washington, D.C., 1992, pp. 63–72.
8. Koutsopoulos, H. N., and A. B. Downey. Primitive-Based Classification of Pavement Cracking Images. *Journal of Transportation Engineering*, ASCE, Vol. 119, No. 3, pp. 402–418, 1993.
9. Chua, K.-M., and L. Xu. Simple Procedure for Identifying Pavement Distress from Video Images. *Journal of Transportation Engineering*, ASCE, Vol. 120, No. 3, pp. 412–431.
10. Pal, S. K., and R. A. King. Image Enhancement Using Smoothing with Fuzzy Sets. *IEEE Transactions on Systems, Man, and Cybernetics*, Vol. 11, No. 7, 1981, pp. 494–501.
11. Pal, S. K. A Note on the Quantitative Measure of Image Enhancement Through Fuzziness. *IEEE Transactions on Pattern Analysis and Machine Intelligence*, Vol. 4, No. 2, 1982, pp. 204–208.
12. Pal, S. K., and A. Ghosh. Fuzzy Geometry in Image Analysis. *Fuzzy Sets and Systems*, Vol. 48, 1992, pp. 23–40.
13. Pal, S. K., and A. Rosenfeld. Image Enhancement and Thresholding by Optimization of Fuzzy Compactness. *Pattern Recognition Letter*, Vol. 7, 1988, pp. 77–86.
14. Pal, S. K., R. A. King, and A. A. Hashim. Image Description and Primitive Extraction Using Fuzzy Sets. *IEEE Transactions on Systems, Man, and Cybernetics*, Vol. 13, No. 1, 1983, pp. 94–100.
15. Keller, J. M., and C. L. Carpenter. Image Segmentation in the Presence of Uncertainty. *International Journal of Intelligent Systems*, Vol. 5, 1990, pp. 193–208.
16. Zhao, Z., X. Li, and H.D. Cheng. An Effective Fuzzy Logic Approach to Image Enhancement. *SPIE Visual Communication and Image Processing*, Vol. 2094, 1993, pp. 244–251.
17. Huntsberger, T. L., C. L. Jacobs, and R. L. Cannon. Iterative Fuzzy Image Segmentation. *Pattern Recognition*, Vol. 18, No. 2, 1985, pp. 131–138.
18. Hu, M.-K. Visual Pattern Recognition by Moment Invariants. *IRE Transactions on Information Theory*, Vol. 8, 1962, pp. 179–187.
19. Noll, R. J. Zernike Polynomials and Atmospheric Turbulence. *Optical Society American Journal*, Vol. 66, No. 3, 1976, pp. 207–211.
20. Reddi, S. S. Radial and Angular Moment Invariants for Image Identification. *IEEE Transactions on Pattern Analysis and Machine Intelligence*, Vol. 3, No. 2, 1981, pp. 240–242.
21. Teague, M. R. Image Analysis via the General Theory of Moments. *Optical Society American Journal*, Vol. 70, No. 8, 1980a, pp. 920–930.
22. Teague, M. R. Optical Calculation of Irradiance Moments. *Applied Optics*, Vol. 19, No. 8, 1980b, pp. 1353–1356.
23. Abu-Mostafa, Y. S., and D. Psaltis. Recognitive Aspective of Moment Invariants. *IEEE Transactions on Pattern Recognition and Machine Intelligence*, Vol. 6, No. 6, 1984, pp. 698–706.
24. Abu-Mostafa, Y. S., and D. Psaltis. Image Normalization by Complex Moments. *IEEE Transactions on Pattern Recognition and Machine Intelligence*, Vol. 7, No. 1, 1985, pp. 46–55.
25. Maitra, S. Moment Invariants. *Proceedings of the IEEE*, Vol. 67, No. 4, 1979, pp. 697–699.
26. Hsia, T. C. A Note on Invariant Moments in Image Processing. *IEEE Transactions on System, Man, and Cybernetics*, Vol. 11, No. 12, 1981, pp. 831–834.
27. Chou, J., W. A. O'Neill, and H. D. Cheng. Evaluation of Pavement Distress Image Using Artificial Neural Networks. accepted by *27th International Symposium on Advance Transportation Applications*, Oct. 31–Nov. 4, 1994a, Aachen, Germany.
28. Chou, JaChing, W. A. O'Neill, and H. D. Cheng. Pavement Distress Classification Using Neural Networks. Presented at *IEEE International Conference on Systems, Man, and Cybernetics*, San Antonio, Tex., 1994.
29. Lindley, C. A., *Practical Image Processing in C*. John Wiley & Sons, Inc., New York, 1991.
30. Belkasim, S. O., M. Shridhar, and M. Ahmadi. Pattern Recognition with Moment Invariants: A Comparative Study and New Results. *Pattern Recognition*, Vol. 24, No. 12, 1991, pp. 1117–1138.

Publication of this report sponsored by Committee on Pavement Monitoring, Evaluation, and Data Storage.